



**HAL**  
open science

# Solidification effects on sill formation: An experimental approach

Lola Chanceaux, Thierry Menand

► **To cite this version:**

Lola Chanceaux, Thierry Menand. Solidification effects on sill formation: An experimental approach. Earth and Planetary Science Letters, 2014, 403, pp.79-88. 10.1016/j.epsl.2014.06.018 . hal-01131784

**HAL Id: hal-01131784**

**<https://hal.science/hal-01131784>**

Submitted on 17 Mar 2015

**HAL** is a multi-disciplinary open access archive for the deposit and dissemination of scientific research documents, whether they are published or not. The documents may come from teaching and research institutions in France or abroad, or from public or private research centers.

L'archive ouverte pluridisciplinaire **HAL**, est destinée au dépôt et à la diffusion de documents scientifiques de niveau recherche, publiés ou non, émanant des établissements d'enseignement et de recherche français ou étrangers, des laboratoires publics ou privés.

1           Solidification effects on sill formation: an experimental approach

2   L. Chanceaux<sup>a,\*</sup>, T. Menand<sup>a,b,c</sup>

3   <sup>a</sup>*Université Blaise Pascal, Laboratoire Magmas et Volcans, F-63000 Clermont-Ferrand, France*

4   <sup>b</sup>*CNRS, UMR 6524, LMV, Clermont-Ferrand, France*

5   <sup>c</sup>*IRD, R 163, LMV, Clermont-Ferrand, France*

---

6   **Abstract**

Sills represent a major mechanism for constructing continental Earth's crust because these intrusions can amalgamate and form magma reservoirs and plutons. As a result, numerous field, laboratory and numerical studies have investigated the conditions that lead to sill emplacement. However, all previous studies have neglected the potential effect magma solidification could have on sill formation. The effects of solidification on the formation of sills are studied and quantified with scaled analogue laboratory experiments. The experiments presented here involved the injection of hot vegetable oil (a magma analogue) which solidified during its propagation as a dyke in a colder and layered solid of gelatine (a host rock analogue). The gelatine solid had two layers of different stiffness, to create a priori favourable conditions to form sills. Several behaviours were observed depending on the injection temperature and the injection rate: no intrusions (extreme solidification effects), dykes stopping at the interface (high solidification effects), sills (moderate solidification effects), and dykes passing through the interface (low solidification effects). All these results can be explained quantitatively as a function of a dimensionless temperature  $\theta$ , which describes the experimental thermal conditions, and a dimensionless flux  $\phi$ , which describes their dynamical conditions. The experiments reveal that sills can only form within a restricted domain of the  $(\theta, \phi)$  parameter space. These experiments demonstrate that contrary to isothermal experiments where cooling could not affect sill formation, the presence of an interface that would be a priori mechanically favourable is not a sufficient condition for sill formation; solidification effects restrict sill formation. The results are consistent with field observations and provide a means to explain why some dykes form sills when others do not under seemingly similar geological conditions.

---

\*Corresponding author. *E-mail address: l.chanceaux@opgc.univ-bpclermont.fr*

7 *Keywords:* sill formation, solidification, rigidity contrasts, analogue modelling

---

## 8 **1. Introduction**

9 Sill intrusions are a major mechanism for constructing continental crust. Indeed, the amalga-  
10 mation of repeated pulses of magma, many of them in the form of sills, can lead to the formation of  
11 magma reservoirs (John, 1988) and plutons as confirmed by geophysical data (Benn et al., 1999),  
12 theoretical models (Annen and Sparks, 2002; Menand, 2008), field studies and geochronological  
13 data (Miller et al., 2011; Horsman et al., 2010; Leuthold et al., 2012). Interconnected sill com-  
14 plexes have also been proposed as viable and efficient pathways for magma transport in the crust  
15 (Cartwright and Hansen, 2006; Muirhead et al., 2012). Thus sills could both lead to magma storage  
16 or its transport in the crust.

17 Different models of sill formation have been proposed based on field observations, laboratory  
18 experiments or numerical simulations: buoyancy could force sills to form at crustal levels where  
19 magmas become neutrally buoyant (Corry, 1988), or could help develop magma overpressures  
20 that are large enough to generate sills along specific horizons (Taisne and Jaupart, 2009); rigidity  
21 anisotropy in the crust could favour sill formation along those interfaces that separate an upper stiff  
22 layer from a softer lower one (Kavanagh et al., 2006; Burchardt, 2008; Maccaferri et al., 2010); rhe-  
23 ology contrast between a ductile rock layer and a brittle one, or between adjacent layers where one  
24 is much more ductile than the other, would favour sill inception between these layers or within the  
25 weakest ductile zones (Parsons et al., 1992; Miller et al., 2011); and stress anisotropy would favour  
26 sill formations in crustal regions with high, horizontal, compressive deviatoric stress (Menand et al.,  
27 2010). An analysis of these different mechanisms suggests that crustal heterogeneities, and their  
28 mechanical or rheological anisotropies, would play a dominant role in controlling whether and  
29 where sills could form (Menand, 2011). However, all these studies have overlooked the potential  
30 effect of magma cooling and solidification.

31 All experimental and numerical studies on sill intrusions have therefore been carried out under  
32 isothermal conditions and have neglected the potential effect of magma solidification on sill for-

33 mation and propagation. In fact, very few studies have dealt with cooling and solidification effects  
34 on intrusions. Theoretical studies (e.g. [Bolchover and Lister, 1999](#); [Lister, 1999](#)) are limited to two  
35 dimensions, and so provide only a limited understanding of solidification effects because intrusions  
36 such as dykes and sills are inherently three-dimensional objects (e.g. [Taisne and Tait, 2009, 2011](#)).  
37 To our knowledge, [Taisne and Tait \(2011\)](#) are the only ones to have investigated experimentally  
38 solidification effects on intrusion propagation, focusing on dykes. They found that solidification  
39 effects have a strong impact on dyke dynamics: when solidification effects are important, dykes  
40 display an intermittent, stepwise mode of propagation, during which dykes momentarily stop prop-  
41 agating and then swell without advancing, before resuming their propagation when the incoming  
42 fluid that is stored in the fissure is able to fracture both the surrounding solid and the frozen crust  
43 that has developed within the fissure. Without solidification, dyke propagation operates continu-  
44 ously. Additionally, solidification affected the propagating dyke by focusing fluid flow in its central  
45 portion, hence limiting its horizontal dimension, and by adding a more complex geometry owing  
46 to the successive and intermittent outbreaks of fluid that occurred around the dyke periphery and  
47 sometimes away from its tip. These findings raise naturally the question of the effects that solidifi-  
48 cation could potentially have not only on the geometry and the dynamics of sills, but also on their  
49 formation.

50 To address this issue, we present laboratory experiments that involved the injection of hot veg-  
51 etable oil (a magma analogue) which solidified during the propagation of an experimental dyke  
52 in a colder and layered solid gelatine (a host rock analogue). The gelatine solid had two layers  
53 of different stiffness, to create a priori favourable conditions to form sills. We investigated ex-  
54 perimentally the effect of solidification on the formation of sills, and quantified how solidification  
55 can restrict sill formation. The experimental approach is introduced in section 2, before presenting  
56 the experimental observations and results in section 3. We discuss their geological implications in  
57 section 4 and then conclude in section 5.

## 58 **2. Experimental approach**

### 59 *2.1. Experimental apparatus*

60 The experiments described here involved the injection of hot vegetable oil (magma analogue)  
61 in a colder gelatine solid inside a tank of  $40 \times 40 \times 40$  cm made of PMMA. The tank had circular  
62 openings of 1 cm diameter at its base to make injections (Fig. 1). The gelatine had two layers with  
63 different stiffness, the upper layer being stiffer than the lower one, to create a priori favourable  
64 conditions to form sills (Kavanagh et al., 2006). The solidification temperature of the vegetable oil  
65 is higher than that of gelatine, which allows the analogue intrusion to partially solidify during its  
66 propagation depending on injection conditions.

67 The injection temperature and the injection flux were controlled and varied between experi-  
68 ments in order to observe the effects of solidification on sill formation. The vegetable oil was  
69 heated with a bain-marie to the desired temperature. This temperature had to be higher than the  
70 solidification temperature of the vegetable oil, which is  $31^\circ\text{C}$  (Galland et al., 2006). The gelatine  
71 was first incised at the base of the tank through the injection point in order to obtain a preferred  
72 orientation for the development of a dyke (the incision was typically 5 cm high). The hot oil was  
73 then injected in the cold gelatine solid through a metal tube of 4 mm diameter that was inserted into  
74 the incision made, and connected to a pipe fed by a peristaltic pump. This pump allowed us to both  
75 control and maintain constant the volumetric injection flux  $Q$  throughout each experiment. The  
76 temperature of the gelatine (host rock) and the injection temperature of the vegetable oil (magma),  
77 measured at the point of injection in the gelatine solid, were continuously recorded throughout the  
78 experiments with thermocouples while the experiments were recorded by a video camera in front  
79 of the tank.

### 80 *2.2. The gelatine*

81 The gelatine used is a 260 bloom, 20 mesh, pig-skin derived gelatine powder prepared in two  
82 batches to obtain a final solid with two layers of the same volume but different stiffness. The  
83 upper layer has to possess a higher stiffness than the lower layer, in order to create mechanically

84 favourable conditions to form sills (Kavanagh et al., 2006). A higher gelatine concentration leads  
 85 to a higher rigidity. The first batch of gelatine was poured in the tank, which was then placed in a  
 86 fridge at a temperature of  $\simeq 5^\circ \text{C}$  for  $\simeq 24$  hours. Once the gelatine was solid, the second batch  
 87 was poured in the tank, which was then placed back in the fridge and kept at the same temperature  
 88 for another  $\simeq 72$  hours before running an experiment.

89 Before running an experiment, measurements of the elastic properties of the gelatine solid were  
 90 performed. The Young's modulus was calculated by applying a cylindrical known-weight load on  
 91 the upper layer of the solidified gelatine and measuring the deflection caused by this load. The  
 92 measured deflection is directly linked to the Young's modulus  $E_{upp}$  of the upper layer (Timoshenko  
 93 and Goodier, 1970):

$$E_{upp} = \frac{Mg(1 - \nu^2)}{Dx} \quad (1)$$

94 where  $M$  is the mass of the applied load in kg;  $g = 9.81 \text{ m.s}^{-2}$  is the gravitational acceleration;  
 95  $\nu = 0.5$  is the Poisson's ratio of the gelatine (Crisp, 1952; Richards Jr and Mark, 1966);  $D$  is the  
 96 diameter of the cylindrical load applied on the gelatine in m;  $x$  is the deflection in m;  $E_{upp}$  is the  
 97 Young's modulus of the upper layer in Pa.

98 To calculate the Young's modulus, the gelatine is assumed to be semi-infinite. To avoid base  
 99 effects and side-wall effects when the load is applied on the gelatine in the tank, the diameter of  
 100 the load needs to be  $\leq 10\%$  of the horizontal dimension of the tank (Kavanagh et al., 2013). In  
 101 these experiments, the applied load measured 29.99 mm in diameter and so represented 7.5% of  
 102 the tank size. The stress variation with depth induced by a load applied to the surface can also be  
 103 calculated. According to Timoshenko and Goodier (1970), the largest stress component induced  
 104 by a load  $\sigma_0$  applied on top of a semi-infinite elastic body is the vertical component  $\sigma_z$ , which can  
 105 be expressed as:

$$\sigma_z = \sigma_0 \left[ 1 - \frac{8z^3}{(1 + 4z^2)^{\frac{3}{2}}} \right] \quad (2)$$

106 where  $z$  is the depth normalized by the load's diameter. The thickness of the gelatine layer was 100

107 mm, so  $z = 3.33$ . Consequently,  $\sigma_z/\sigma_0 = 3.3 \%$ . The vertical stress generated by the surface load  
 108 at 10 cm depth in a semi-infinite elastic medium would be only 3.3 % of the surface load. This  
 109 allowed us to assume that the base and side-wall had negligible effects, and to consider the upper  
 110 gelatine layer as a semi-infinite medium, and equation (1) to be valid.

111 The formation of a sill requires that the Young's modulus of the upper layer  $E_{upp}$  is higher  
 112 than the Young's modulus of the lower layer  $E_{low}$ . It is not possible to directly measure  $E_{low}$ , but  
 113 the Young's modulus ratio between the two layers can be easily calculated as a first approximation  
 114 from the Young's modulus ratio at infinite time,  $\Delta E = E_{upp}/E_{low}$ , provided the gelatine layers  
 115 are left long enough to solidify. Indeed, the Young's modulus of the gelatine increases with time  
 116 before reaching a plateau  $E_\infty$  after about 48 hours, although the exact amount of time depends on  
 117 the gelatine concentration and volume (Kavanagh et al., 2013). Therefore, the gelatine layers were  
 118 left long enough before running an experiment to ensure they had reached their Young's modulus  
 119 plateaus  $E_{upp\infty}$  and  $E_{low\infty}$  (72 to 96 hours) and that the Young's modulus ratio had reached the  
 120 constant value:

$$\Delta E = \frac{E_{upp\infty}}{E_{low\infty}} = \frac{\alpha w_{upp} + \beta}{\alpha w_{low} + \beta} = \frac{w_{upp} - 1.3}{w_{low} - 1.3} \quad (3)$$

121 where  $w$  is the concentration by weight of the upper and lower layers; the numerical constants  $\alpha$   
 122 and  $\beta$  have been estimated to be  $\alpha = 6000$  and  $\beta = -7800$  (Kavanagh et al., 2013). This ratio  
 123 allows the value  $E_{low}$  of the lower layer to be calculated once  $E_{upp}$  has been determined. This  
 124 measurement method for the Young's modulus has the added advantage of ensuring that the time  
 125 between the preparation of the two layers is kept to a minimum, which helps to create an interface  
 126 between the two that is as strong as possible.

127 Our experiments were designed to investigate and quantify the potential effect fluid solidifica-  
 128 tion could have on sill formation when mechanically favourable conditions are already met. As  
 129 shown by Kavanagh et al. (2006) isothermal experiments, sills should always occur when the rigid-  
 130 ity contrasts  $\Delta E > 1.1$ . We therefore ran all our experiments in this mechanical condition and  
 131 deliberately chose as narrow a  $\Delta E$  range as possible to isolate and quantify the effect of solidifica-

132 tion. The rigidity contrast  $\Delta E$  in our experiments lied between 1.4 and 3.9.

### 133 2.3. *Experimental limitations*

134 Several assumptions were made in the experiments reported here. One limitation concerns  
135 a parameter that is unknown and uncontrolled in the experiments: the strength of the interface,  
136 i.e. how strongly welded the interface is. If an interface is weak or even not welded, it will  
137 necessarily force the creation of a sill, regardless of the rigidity contrast. This parameter will  
138 affect the formation of sills. In the experiments reported here, the interface is considered welded  
139 and relatively strong, but how strong is not known. This difficulty is inherent to an experimental  
140 approach, and quantifying the impact of interface strength on sill intrusions is more likely to be  
141 resolved by numerical studies.

142 Also, gelatine has an elastic behaviour and cannot act as an analogue material to simulate non-  
143 elastic behaviour of the crust. However, restricting our investigation to the elastic case, enabled  
144 us to focus on the effect solidification could have on sill formation, and to be able to compare our  
145 results with previous studies, which were also elastic. Moreover, even though rocks of the Earth's  
146 crust are fractured and heterogeneous, the elastic approximation has been shown to be appropriate  
147 to first order ([Delaney and Pollard, 1981](#)).

148 Finally, the state of stress is considered lithostatic (or "gelistatic"), so these experiments are not  
149 applicable to different stress environments (e.g. tectonic stresses, stresses induced by the load of a  
150 volcanic edifice, ...).

### 151 2.4. *Data processing*

152 To analyse the experiments, we follow the experimental analysis of [Taisne and Tait \(2011\)](#) and  
153 define two dimensionless parameters. One describes the thermal conditions of the experiments at  
154 the injection point (dimensionless temperature  $\theta$ ) and the other describes their dynamical condi-  
155 tions (dimensionless flux  $\phi$ ).

156 The dimensionless temperature  $\theta$  is defined as:

$$\theta = \frac{(T_s - T_g)}{(T_i - T_g)} \quad (4)$$



157 where  $T_s$  is the solidification temperature of vegetable oil,  $T_s = 31^\circ \text{ C}$  (Galland et al., 2006);  $T_g$   
 158 is the gelatine temperature during the injection, typically between  $5$  and  $7^\circ \text{ C}$ ;  $T_i$  is the injection  
 159 temperature of vegetable oil. We note that  $\theta$  can only be defined mathematically if the three tem-  
 160 peratures differ from one another. This will not be the case if the injection temperature is equal to  
 161 the gelatine ambient temperature as this would amount to having also the solidification tempera-  
 162 ture equal to the two other temperatures. In this particular case, trying to define a dimensionless  
 163 temperature theta would therefore be meaningless.

164 The dimensionless flux  $\phi$  is defined as the ratio between the heat advected by vegetable oil and  
 165 the heat lost by conduction in the gelatine.  $\phi$  describes the competition between the heat advected  
 166 along the intrusion over a time  $\Delta t$  to increase the temperature by an amount  $\Delta T$  and the heat  
 167 lost by conduction over a distance  $\delta$  and the same time  $\Delta t$ . The advected heat  $A$  is defined by  
 168  $A = \rho H L B C_p \frac{\Delta T}{\Delta t} = Q \rho C_p \Delta T$  where  $\rho$  is the density of the intrusion;  $H$  is the thickness,  $L$  the  
 169 length, and  $B$  the breadth of the intrusion;  $C_p$  is the heat capacity of the intrusion;  $Q = V/\Delta t$   
 170 is the flux, or volumetric rate of flow of the intrusion where  $V = H L B$  is its volume. The heat  
 171 lost by conduction  $C$  is defined by  $C = \rho H L B C_p \frac{\Delta T}{\Delta t}$  which diffuses over a distance  $\delta$  in a time  
 172  $\Delta t = \delta^2/\kappa$  where  $\kappa$  is the thermal diffusivity. In the experiments presented here, the heat lost by  
 173 conduction is considered to be over a distance similar to the thickness of the intrusion, i.e.  $\delta \simeq H$ .  
 174 Therefore:  $C = \frac{\rho H L B C_p \Delta T \kappa}{H^2} = \frac{\rho L B C_p \Delta T \kappa}{H}$ . And we get the dimensionless flux:

$$\phi = \frac{A}{C} = \frac{QH}{\kappa LB} \quad (5)$$

175 To find  $H/LB$ , a pressure balance is used (Taisne and Tait, 2011) between the buoyancy  
 176 pressure  $P_b$ , that drives the intrusion, and the elastic pressure  $P_e$ , which allows the dyke to deform  
 177 the host rock:

$$P_b = P_e \Rightarrow \Delta \rho g L = \frac{E}{2(1-\nu^2)} \frac{H}{B} \Leftrightarrow \frac{H}{LB} = \frac{2(1-\nu^2)}{E} \Delta \rho g \quad (6)$$

178 where  $\Delta \rho$  is the density difference between the host rock and the intrusion;  $g = 9.81 \text{ m.s}^{-1}$  is  
 179 the gravitational acceleration;  $E$  and  $\nu$  are the Young's modulus and the Poisson's ratio of the host  
 180 rock.

181 The same formula as in [Taisne and Tait \(2011\)](#) is found for the dimensionless flux of a dyke:

$$\phi = \frac{3Q\Delta\rho g}{2E\kappa} \quad (7)$$

182 where  $Q$  is the flux of injection in  $\text{m}^3 \cdot \text{s}^{-1}$ ;  $\Delta\rho$  is the difference of density between the gelatine  
 183 and the vegetable oil - from [Galland et al. \(2006\)](#),  $\rho_{vegetableoil} = 892 \text{ kg} \cdot \text{m}^{-3}$  and  $\rho_{gelatine} = 1000$   
 184  $\text{kg} \cdot \text{m}^{-3}$  (considered the same as that of water) therefore  $\Delta\rho = 108 \text{ kg} \cdot \text{m}^{-3}$ ;  $E$  is the Young's  
 185 modulus of the lower layer (through which the dyke propagates);  $\nu = 0.5$  is the gelatine Poisson's  
 186 ratio;  $\kappa$  is the thermal diffusivity (assumed to be identical to that of water),  $\kappa = 1.4 \times 10^{-7} \text{ m}^2 \cdot \text{s}^{-1}$ ;  
 187  $g = 9.81 \text{ m} \cdot \text{s}^{-2}$  is the gravitational acceleration.

188  $T_s$  and  $T_g$  were essentially the same for all experiments so  $\theta$  varied only with  $T_i$  the injection  
 189 temperature. Likewise,  $\Delta\rho$ ,  $g$ ,  $\kappa$  were all kept constant. Consequently,  $\phi$  varied between experi-  
 190 ments with the injection flux  $Q$  and the Young's modulus  $E_{low}$  of the lower layer.  $\theta$  and  $\phi$  were  
 191 maintained constant during an experiment ( $T_i$ ,  $E_{low}$  and  $Q$  were maintained constant), and were  
 192 varied systematically between experiments to quantify their respective influence on the formation of  
 193 sills.

194  $\theta$  varies between 0 and 1 and  $\phi$  varies between 0 and  $\infty$ . [Table 1](#) summarises the behaviour of  
 195  $\theta$  and  $\phi$ .

$\theta \rightarrow 1$	$T_i \rightarrow T_s$	solidification operates rapidly
$\theta \rightarrow 0$	$T_i \gg T_s$	almost no solidification
$\phi \rightarrow 0$	low $Q$ values	solidification operates rapidly
$\phi \gg 1$	high $Q$ values	almost no solidification

Table 1: Behaviour of the dimensionless temperature  $\theta$  and dimensionless flux  $\phi$ .

## 196 2.5. Experimental strategy

197 The flux  $\phi$  and the temperature  $\theta$  are dimensionless. These values are thus scale-independent,  
 198 and can be compared between experiments and with values in nature.

199 Regarding  $\theta$ , in the Earth's crust, values of  $300^\circ\text{ C}$  at  $\simeq 10\text{ km}$  depth and  $450^\circ\text{ C}$  at  $\simeq 15\text{ km}$   
200 depth are obtained (using a thermal gradient of  $30^\circ\text{ C.km}^{-1}$ ) for the temperature of the host rock  
201 ( $T_g$ ). Magmatic injection and solidification temperatures will depend on magma composition: for  
202 a basalt, reasonable values are  $T_i \simeq 1200^\circ\text{ C}$  and  $T_s \simeq 900^\circ\text{ C}$  while for a rhyolite,  $T_i \simeq 800^\circ\text{ C}$   
203 and  $T_s \simeq 775^\circ\text{ C}$ . Using equation (4), the range of natural values obtained for  $\theta$  is:

- 204 •  $\theta = 0.67$  (basalt) to  $\theta = 0.95$  (rhyolite) at  $10\text{ km}$  depth;
- 205 •  $\theta = 0.60$  (basalt) to  $\theta = 0.93$  (rhyolite) at  $15\text{ km}$  depth.

206 Regarding  $\phi$ , Taisne and Tait (2011) used as natural values  $E \simeq 10\text{ GPa}$ ,  $\kappa \simeq 10^{-6}\text{ m}^2.\text{s}^{-1}$  and  
207  $\Delta\rho \simeq 100\text{ kg.m}^{-3}$ . The range of magmatic flux  $Q$  is quite large, but values between 1 and 100  
208  $\text{m}^3.\text{s}^{-1}$  seem to be typical of many volcanoes, including Piton de la Fournaise Volcano, La Réunion  
209 Island, France (Traversa et al., 2010). Of course, these values could be extended. Indeed, magmatic  
210 fluxes can reach values higher than  $1000\text{ m}^3.\text{s}^{-1}$ , i.e. an order of magnitude higher, as has been  
211 observed at the Mauna Loa in Hawaii or during the 1783 Laki eruption in Iceland (Macdonald and  
212 Finch, 1950; Thordarson and Self, 1993). However this is rather an exception, and values between  
213 1 and  $100\text{ m}^3.\text{s}^{-1}$  seem more reasonable. Using equation (7), the range of natural values obtained  
214 for  $\phi$  is:

- 215 •  $\phi = 0.15$  ( $Q \simeq 1\text{ m}^3.\text{s}^{-1}$ ) to  $\phi = 16$  ( $Q \simeq 100\text{ m}^3.\text{s}^{-1}$ ).

216 In order to scale experiments correctly, the range of experimental injection temperatures and fluxes  
217 were chosen to ensure they cover these ranges of natural values for  $\theta$  and  $\phi$ . The experiments  
218 focused on the formation of sills in experiments involving solidification. Therefore  $\theta$  and  $\phi$  were  
219 varied systematically between experiments to identify whether these values affected conditions for  
220 the formation of sills and the type of the intrusions (feeder dykes or sills).

## 221 2.6. Scaling

222 If the experiments reported here represent a good analogue of natural intrusions, they should be  
223 correctly scaled so that their geometry, kinematics and dynamics are similar to those in nature. The

224 scaling procedure for analogue intrusions defined in [Kavanagh et al. \(2013\)](#) is followed. Different  
 225 scale ratios between experimental parameters and natural parameters are defined:

$$L^* = \frac{L_l}{L_n}; \quad T^* = \frac{T_l}{T_n}; \quad U^* = \frac{U_l}{U_n}; \quad E^* = \frac{E_l}{E_n} \quad (8)$$

226 where the subscript  $l$  means laboratory and the subscript  $n$  means nature, so that  $*$  is the ratio  
 227 between the value measured in laboratory experiments and the natural value.  $L$  is a length scale,  $T$   
 228 is a time scale,  $U$  is a velocity scale and  $E$  is a Young's modulus scale.

229 The characteristic length scale of a dyke is the buoyancy length  $L_b$  ([Taisne and Tait, 2011](#)).  
 230 It is the length, for which the buoyancy pressure (allowing the ascent of the dyke) is balanced by  
 231 resistance from rock fracture, and defined as:

$$L_b = \left( \frac{K_c}{\Delta\rho g} \right)^{\frac{2}{3}} \quad (9)$$

232  $K_c$  is the fracture toughness;  $\Delta\rho$  is the density difference between the host rock and the fluid;  
 233  $g = 9.81 \text{ m.s}^{-2}$  is the gravitational acceleration.

234 By introducing the reduced gravity scale  $g' = \Delta\rho/\rho_{solid}$  where  $\rho_{solid}$  is the density of the host  
 235 rock, a characteristic time scale  $T$  and a characteristic velocity scale  $U$  can be defined:

$$T = \sqrt{\frac{L_b}{g'}}; \quad U = \frac{L_b}{T} \quad (10)$$

236 To obtain a characteristic Young's modulus scale, a balance between the buoyancy pressure  
 237 ( $\Delta\rho g L_b$ ) and the elastic pressure  $\left( \frac{E}{2(1-\nu^2)} \frac{H}{L_b} \right)$  that occurs in the head region of the dyke is used,  
 238 yielding the following scale:

$$E = 2(1-\nu^2) \Delta\rho g L_b \frac{L_b}{H} \quad (11)$$

239 where  $H$  is the thickness of the dyke head;  $E$  is the Young's modulus of the surrounding solid,  
 240 and  $\nu$  its the Poisson's ratio ([Kavanagh et al., 2013](#)). Moreover,  $\nu = 1/2$  for gelatine and  $\nu = 1/4$

241 - 1/3 for rocks therefore  $2(1 - \nu^2)$  does not vary much between the laboratory and nature. From  
 242 these expression we obtain:

$$L^* = \left( \frac{K_c^*}{\Delta\rho^*} \right)^{\frac{2}{3}} \quad (12)$$

$$243 \quad T^* = (\rho_{solid}^*)^{\frac{1}{2}} (K_c^*)^{\frac{1}{3}} (\Delta\rho^*)^{-\frac{5}{6}} \quad (13)$$

$$244 \quad U^* = (\rho_{solid}^*)^{-\frac{1}{2}} (K_c^*)^{\frac{1}{3}} (\Delta\rho^*)^{\frac{1}{6}} \quad (14)$$

$$245 \quad E^* = \Delta\rho^* L_b^* \left( \frac{L_b}{H} \right)^* \quad (15)$$

246 In our experiments,  $E_{l_{mean}} \simeq 5000$  Pa implying a fracture toughness  $K_c \simeq 100$  Pa.m<sup>1/2</sup>  
 247 (Kavanagh et al., 2013). These values give us an experimental buoyancy length  $L_b \simeq 22$  cm.

248 In nature,  $K_c$  varies between 10<sup>6</sup> to 10<sup>8</sup> Pa.m<sup>1/2</sup> depending on whether the value is measured  
 249 in the field or in the laboratory (Delaney and Pollard, 1981).  $K_c \simeq 10^7$  Pa.m<sup>1/2</sup> seems to be a  
 250 representative value. The ratio between thickness and length  $H/L_b$  for a dyke varies in nature  
 251 between 10<sup>-4</sup> and 10<sup>-3</sup> (Kavanagh and Sparks, 2011; Gudmundsson, 2011), while it is  $\simeq 10^{-2}$  -  
 252 10<sup>-1</sup> in gelatine. The magnitude of  $\Delta\rho$  in nature is 100 kg.m<sup>-3</sup>, i.e. the same as in gelatine. Finally,  
 253 we take a value for  $\rho_{solid}$  of 2800 kg.m<sup>-3</sup> in nature and 1000 kg.m<sup>-3</sup> in gelatine. Consequently:

$$254 \quad \bullet \quad L^* = 4.6 \times 10^{-4}$$

$$255 \quad \bullet \quad T^* = 1.3 \times 10^{-2}$$

$$256 \quad \bullet \quad U^* = 3.6 \times 10^{-2}$$

$$257 \quad \bullet \quad E^* = 10^{-5} - 10^{-7}$$

258 With experimental values  $L_l = L_b \simeq 22$  cm,  $T_l \simeq 80 - 400$  s,  $U_l \simeq 7$  mm.s<sup>-1</sup> and  $E_l = E_{l_{mean}} \simeq$   
 259 5000 Pa, these give:

$$260 \quad \bullet \quad L_n = 480 \text{ m, which seems reasonable;}$$

$$261 \quad \bullet \quad T_n = 2 - 9 \text{ h, which seems also reasonable;}$$

- 262 •  $U_n = 0.2 \text{ m.s}^{-1}$ , which is consistent with velocity of dykes between 0.1 and  $0.5 \text{ m.s}^{-1}$   
 263 ([White et al., 2011](#));
- 264 •  $E_n = 10^9 - 10^{11} \text{ Pa}$ , which are typical natural values.

265 These calculations confirm that the experiments are correctly scaled.

266 In addition to the scale ratios determined by [Kavanagh et al. \(2013\)](#), we define an additional  
 267 characteristic dynamic flux scale. A natural flux scale is:

$$Q = HL_bU \quad (16)$$

268 and applying the same pressure balance between the buoyancy pressure and the elastic pressure in  
 269 the dyke head region as before - equation (11) - yields the following expression for the thickness  
 270  $H$ :

$$H = \Delta\rho g (L_b)^2 \frac{2(1-\nu^2)}{E} \quad (17)$$

271 Consequently:

$$Q^* = \Delta\rho^* (L^*)^3 (E^*)^{-1} U^* \\ \Rightarrow Q^* = 10^{-7} - 10^{-5} \quad (18)$$

273 Experimental fluxes  $Q_l$  have typical values of  $10^{-7}$  to  $10^{-5} \text{ m}^3.\text{s}^{-1}$ , which would correspond  
 274 to natural values  $Q_n = 0.01 - 100 \text{ m}^3.\text{s}^{-1}$ , which are similar to natural values for volcanic systems  
 275 (e.g. [Traversa et al., 2010](#)). We note that this range of natural flux  $Q_n$  is deduced directly from  
 276 a scaling argument and therefore it does not include any considerations of the thermal evolution  
 277 of the intrusion. It is thus independent from the range of flux considered to calculate the range  
 278 of dimensionless fluxes  $\phi$  in section 2.5. The range of fluxes in the experiments thus correctly  
 279 represent the dynamics of natural intrusions ( $Q_n$ ), and their thermal evolution ( $\phi$ ).

280 **3. Results**

281 Fifteen experiments were performed with different injection temperatures and injection fluxes  
 282 (Tab. 2). For each experiment,  $\theta$  and  $\phi$  were calculated.  $\phi$  quantified the dyke dynamical conditions  
 283 in the lower layer, and thus whether conditions for sill formation could be met.

Exp	$w_{upp}$	$w_{low}$	$T_g(C)$	$T_i(C)$	$E(Pa)$	$Q(m^3.s^{-1})$	$\theta$	$\phi$	$\frac{\sigma_\theta}{\theta}$	$\frac{\sigma_\phi}{\phi}$	Result	Symbols
1	5	3	7.00	45.78	10164	1.38E-06	0.62	1.54	0.03	0.08	Sill	●
2	5	3	7.02	46.02	10164	2.50E-06	0.62	2.79	0.03	0.07	Crossing dyke	△
3	3	2	7.56	42.65	996	1.38E-06	0.67	15.68	0.04	0.07	Crossing dyke	△
4	3	2	5.73	44.08	3159	3.75E-06	0.66	13.48	0.03	0.06	Crossing dyke	△
5	4	2	5.87	38.35	2930	2.50E-06	0.77	9.69	0.04	0.06	Sill	●
6	4	2	6.24	34.81	2882	2.50E-06	0.87	9.85	0.04	0.06	Blocked dyke	□
7	4	2	6.24	34.81	2882	4.00E-06	0.87	15.77	0.04	0.06	Sill	●
8	4	2	6.64	32.44	1828	2.25E-06	0.94	13.98	0.04	0.06	Blocked dyke	□
9	4	2	6.64	32.44	1828	7.51E-07	0.94	4.66	0.04	0.09	No intrusion	★
10	5	4	6.66	37.72	12903	1.50E-05	0.78	13.21	0.04	0.06	Sill	●
11	5	4	6.66	37.72	12903	1.00E-06	0.78	0.88	0.04	0.08	No intrusion	★
12	4	2	6.57	43.34	3003	2.50E-06	0.66	9.96	0.04	0.15	Sill	●
13	4	2	6.57	43.34	2851	1.38E-06	0.66	5.48	0.03	0.07	Sill	●
14	4	2	6.57	40.89	2851	3.75E-07	0.71	1.42	0.03	0.06	Blocked dyke	□
15	4	2	6.48	37.07	3003	2.00E-06	0.80	7.57	0.04	0.07	Sill	●

Table 2: Experimental data for investigation of sill formation.

$\theta$  is calculated from equation (4) with  $T_s = 31^\circ C$ .  $\phi$  is calculated from equation (7) with  $\Delta\rho = 100$ ,  $g = 9.81 m.s^{-1}$ ,  $\kappa = 1.4 \times 10^{-7} m^2.s^{-1}$ .  $E$  of the lower gelatine layer is determined and calculated from equation (3). The uncertainties  $\sigma_\theta$  and  $\sigma_\phi$  were calculated according to the principles of the "Propagation of Errors" (Bevington and Robinson, 2003).

284 In all experiments, a dyke was first generated in the lower layer. All experiments were pre-  
 285 pared in such a way that the interface between the two gelatine layers was a priori mechanically  
 286 favourable for the formation of sills ( $\Delta E > 1.1$  - Kavanagh et al., 2006). However, contrary to  
 287 what has been observed in previous isothermal experimental studies (e.g. Kavanagh et al., 2006),  
 288 sill formation did not systematically occur. Instead, different types of intrusion were observed:

289 dykes blocked at the interface, dykes passing through the interface, and sills. Each type of intru-  
290 sion could be linked to distinct  $\theta$  and  $\phi$  fields.

### 291 *3.1. Types of intrusions*

292 The initial dyke could be blocked at the interface (Fig. 2A). It stopped its vertical propagation  
293 there and propagated laterally, underneath the interface, until the end of the injection (Fig. 3C).  
294 These dykes were particularly thick with a thickness to length ratio greater than  $10^{-1}$ .

295 When a sill formed (Fig. 2B) it took place at the interface between the two layers. Initially, the  
296 feeder dyke propagated in the same way as a dyke blocked at the interface before fracturing and  
297 propagating parallel to the interface, forming a sill (Fig. 3D). During the propagation of a sill, the  
298 upper layer was deformed and the interface bulged slightly towards the surface.

299 The dyke could also pass through the interface (Fig. 2C). It propagated initially in the same way  
300 as a dyke blocked at the interface before piercing the interface and propagating into the upper stiffer  
301 layer (Fig. 3E). The dyke made a pause before penetrating the interface and taking a triangular  
302 shape along strike above the interface. These dykes had a thickness to length ratio of  $\simeq 10^{-1}$  (the  
303 length used is the total vertical length of the dyke in the lower and upper layer).

### 304 *3.2. Morphologies of intrusions*

305 Different morphologies of intrusions were observed, all similar to those observed in nature.  
306 The experimental dykes had sometimes a smooth surface, but were usually very irregular. Plumose  
307 structures were commonly observed (Fig. 4A). Additionally, many discontinuities could be seen at  
308 the leading edges of the experimental dykes as en-echelon segments (Fig. 4B) or lobes (Fig. 4C).  
309 These en-echelon segments did not always have the same orientation. The discontinuities observed  
310 on our experimental dykes are similar to those observed in [Taisne and Tait \(2011\)](#) and they are  
311 linked to solidification processes. We observe that for dykes and sills as solidification effects  
312 become more important, the number of discontinuities usually increases as well. Additionally,  
313 these discontinuities are not limited to the propagating tip of the fissure but are also initiated at  
314 the margins (e.g. Fig. 4C), which corroborates the observations of [Taisne and Tait \(2011\)](#). In



315 comparison, the experimental sills had generally very smooth surfaces with few asperities filled  
316 with gelatine (Fig. 4D). The surface of the sills were smooth probably because they did not really  
317 need to fracture the gelatine in order to propagate along the interface. However, as for dykes,  
318 discontinuities were also observed at the edge of some (Fig. 4E).

### 319 3.3. Result analysis

320 The results of the experiments, that is blocked dykes, crossing dykes, sills and cases when fluid  
321 could not intrude the gelatine, are all summarised on a graph showing  $\theta$  as a function of  $\phi$  (Fig. 5).  
322 Solidification effects increase as  $\theta \rightarrow 1$  and  $\phi \rightarrow 0$ . Four areas are clearly identified:

- 323 • when the dimensionless temperature is relatively high and the dimensionless flux is very low  
324 ( $\theta \simeq 0.75 - 0.95$  and  $\phi < 6$ ), there is no propagation (Fig. 5, stars). Solidification effects are  
325 so important that vegetable oil freezes and solidifies in the tube and no intrusion is observed;
- 326 • when the dimensionless temperature is high and for larger dimensionless fluxes ( $\theta \simeq 0.7 -$   
327  $0.95$  and  $\phi < 15$ ), dykes are blocked at the interface between the two gelatine layers (Fig.  
328 5, squares). Solidification effects are important and the dyke partially solidifies at its walls  
329 during its propagation and development. Solidification at the upper tip of the dyke blocks  
330 its propagation, and prevent its piercing of the interface and subsequent propagation in the  
331 upper stiffer layer or its spreading along the interface as a sill;
- 332 • when the dimensionless temperature has intermediate values ( $\theta \simeq 0.60 - 0.90$  and  $\phi < 16$ ),  
333 sills are created (Fig. 5, disks). Solidification effects are smaller. Consequently, the feeder  
334 dyke propagates as a sill by spreading at the interface between the two layers;
- 335 • finally, when the dimensionless temperature is low ( $\theta \simeq 0.60 - 0.70$  and  $\phi > 2$ ), dykes  
336 passing through the interface are created (Fig. 5, triangles). Dykes do not create sills but  
337 instead pierce directly the interface to propagate in the upper layer, easily fracturing the  
338 gelatine presumably because of their high temperature: higher input of hot vegetable oil at the  
339 tip of the feeder dyke leads to lower solidification effects and presumably easier fracturation;

340 the injection flux seemed to have less of an effect. However, solidification along the walls of  
341 the dyke seem to prevent the fluid from intruding the interface between the gelatine layers.

342 These results are consistent and systematic over the narrow range of rigidity contrasts  $\Delta E$  used  
343 in the experiments ( $1.4 \leq \Delta E \leq 3.9$ ).

## 344 4. Discussion

### 345 4.1. Sill Formation

346 The first important result of our experiments is the difference with isothermal experiments  
347 (using water as the injected fluid) where there is no effect of solidification. Indeed, in these ex-  
348 periments (Kavanagh et al., 2006), sill formation occurred systematically when the upper gelatine  
349 layer was stiffer than the lower one. With solidification effects, the rigidity contrast alone is not  
350 sufficient anymore to ensure sill formation. The conditions that are required for the formation of  
351 sills are reduced: it becomes more difficult to form sills when solidification of the flowing fluid  
352 occurs. At a given intermediate value of the dimensionless temperature  $\theta$ , dykes passing through  
353 the interface are created for higher values of the dimensionless flux  $\phi$  whereas sills are created  
354 with lower  $\phi$  values (i.e. lower injection flux  $Q$ ). In the same way at a comparatively higher value  
355 of  $\theta$ , sills are created for higher values of  $\phi$  and dykes blocked at the interface are created at  $\phi$   
356 comparatively lower  $\phi$  values.

357 Each type of intrusion corresponds to a well defined area in Fig. 5, and so to a specific range of  
358  $\theta$  and  $\phi$  values. The limits of each area appear well defined by the following linear relationships:

359 • (b):  $\theta = 0.019\phi + 0.68$  ( $R^2 = 0.99$ );

360 • (c):  $\theta = 0.0039\phi + 0.61$  ( $R^2 = 0.89$ ).

361 These two equations (b) and (c) delimit the upper and lower ranges, respectively, of thermal ( $\theta$ ) and  
362 dynamical ( $\phi$ ) conditions for the formation of sills. It seems that there is also a separation between  
363 the "no propagation" area and the "dyke blocked at the interface" area (dashed line on Fig. 5),

364 but this separation (a) is only qualitative. Sill formation depends on the thermal and dynamical  
365 conditions of the injected fluid. The thermal conditions ( $\theta$ ) depends essentially on the injection  
366 temperature  $T_i$  whereas the dynamical conditions ( $\phi$ ) depends not only on the injection flux  $Q$   
367 but also on the rigidity of the intruded solid. Therefore, the formation of sills in our experiments  
368 depends mainly on three parameters: the rigidity of the rocks intruded below a potential interface,  
369 the injection temperature  $T_i$ , and the injection flux  $Q$ .

#### 370 4.2. Geological Applications

371 These experiments were carried out under dimensionless conditions ( $\theta$  and  $\phi$ ) identical to those  
372 present in nature. The experimental results can therefore be extended to natural conditions. These  
373 results imply that because of solidification effects, even if mechanical conditions are favourable  
374 (upper layer stiffer than the lower one), above some injection magmatic flux (equation (c), Fig. 5),  
375 sills are no longer created, and dykes passing through the interface are expected instead, which  
376 could lead to an eruption.

377 The experimental results provide also a means to explain why some dykes form sills when  
378 other dykes do not under seemingly similar geological conditions. If one considers a dyke that  
379 encounters an interface with favourable mechanical conditions (rigidity contrast with  $\Delta E > 1.1$ ),  
380 different scenarios can be envisaged depending on its dynamical and thermal conditions (Fig. 5).  
381 If conditions for sill formation were met (favourable injection temperature and flux), a sill would  
382 be created. However, a recharge in magma (e.g. the arrival of a new magma batch) or a new  
383 dyke propagating with a higher flux would change the dynamical and thermal conditions owing to  
384 increased magmatic flux and/or injection temperature. The conditions for sill formation would no  
385 longer be met and the dykes would now be able to cross the interface. In the same way, if a dyke  
386 was blocked at an interface because conditions for sill formation were not met (too low injection  
387 temperature or flux) a sill could subsequently form because of a recharge in magma, which would  
388 lead to a temperature and flux increase. Similarly, if a dyke crossed the interface because of a large  
389 injection temperature or flux, this dyke could later turn into a sill along a subsequent favourable  
390 mechanical interface. As magma flows, it cools down and its injection flux will likely decrease as

391 magma is withdrawn from the source: thermal and dynamical conditions will change and increase  
392 the likelihood for sill formation further away.

393 These results are consistent with field observations. Indeed, sills are not created each time there  
394 is a suitable rigidity contrast (upper layer stiffer than the lower one) as illustrated in Fig. 6 where a  
395 feeder dyke crosses several interfaces in the same rock unit, and thus characterised by presumably  
396 similar rigidity contrast, before spreading as a sill at one of them. Solidification effects could be a  
397 plausible explanation for this behaviour.

398 Our experiments explored a limited range of dimensionless fluxes  $\phi$  when extremely-high-flux  
399 dykes do sometimes occur in nature, with  $\phi$  values perhaps as high as 200. Extrapolating the results  
400 summarised in Fig. 5 to high values suggests that dykes with extremely-high dimensionless flux  
401 would have a greater propensity for crossing interfaces and thus for getting closer to the surface.  
402 Although this makes sense, our results might not necessarily hold for such extreme events, and  
403 additional work should clarify the behaviour of these extremely-high-flux dykes.

404 Additionally, some issues could not be addressed with our experiments. First, these experi-  
405 ments assume the deformation of the host rock is elastic. If materials are not consolidated (pyro-  
406 clastic flows, hyaloclastites, shales, ...), deformation can be ductile, which would affect the forma-  
407 tion of sills (very weak interface because of very soft material, premature arrest of the feeder dyke  
408 ...). These interactions with non-elastic materials are expected to be more important for intrusions  
409 close to the surface because crustal heterogeneities are likely to be more important there.

410 Another issue is that these experiments study the effects of solidification on the magma but  
411 neglect the potential effect on the host rocks. The temperature difference between the host rock and  
412 the intrusion and the heat advected by the intrusion during its propagation may affect the rheology  
413 of the host rock. For example, if an intrusion is taking place near an area of magma storage, the  
414 crust heated by this presence could possess a different rheology, likely to be more ductile than  
415 elastic.

416 Also, the vegetable oil used as a magma analogue here has a single solidification temperature.  
417 Magma in nature will have a range of solidification temperature between its liquidus and solidus.

418 This temperature range depends widely on its composition, which evolves as the magma solidifies.  
419 Likewise, the experimental temperature at the injection point  $T_i$  was maintained constant during an  
420 experiment whereas magma temperature is likely to change during an intrusive event. In nature the  
421 thermal conditions  $\theta$  are thus likely to change, which is not accounted for in these experiments. In  
422 the same way,  $\phi$  remains constant during an experiment because  $Q$  is maintained constant whereas  
423 natural magma fluxes are likely to wax and wane during the same injection of magma.

## 424 5. Conclusions

425 The purpose of this study was the quantification of the effects of solidification on the formation  
426 of sills by means of analogue laboratory experiments. They involved the injection of hot vegetable  
427 oil, a magma analogue that solidifies during its injection, in a layered colder solid gelatine, a host  
428 rock analogue. The injection temperature  $T_i$  and the injection flux  $Q$  were systematically varied  
429 between experiments. The experiments were carried out under dimensionless conditions (temper-  
430 ature  $\theta$  and flux  $\phi$ ) identical to those present in nature, and are correctly scaled geometrically,  
431 dynamically, kinematically, and thermally. The results are consistent with field observations and  
432 provide a means to explain why some dykes form sills where other dykes do not under similar  
433 geological conditions.

434 Several types of intrusions were observed: dykes stopping at the interface, dykes passing  
435 through the interface and sills. These different shapes demonstrate that contrary to isothermal  
436 experiments (no temperature effect able to block sill formation), a rigidity contrast between two  
437 layers is not a sufficient condition to create a sill. When solidification effects are significant (low  
438  $Q$  and  $T_i$  slightly higher than  $T_s$ ), the created dyke partially solidifies on the walls during its prop-  
439 agation, which prevents its piercing of the interface and propagation in the upper stiffer gelatine  
440 layer, or its spreading along the interface as a sill. When solidification effects are lower (range  
441 of medium  $Q$  and  $T_i$  higher than  $T_s$ ), the feeder dyke can propagate as a sill by spreading at the  
442 interface between the two layers. When solidification effects are low (range of medium and high  
443  $Q$  and  $T_i$  higher than  $T_s$ ), the constant input of hot vegetable oil at the dyke tip allows it to pierce

444 the interface and propagate in the upper layer of gelatine.

445 Thus, solidification effects restrict sill formation at an interface with a favourable rigidity con-  
446 trast (upper layer stiffer than the lower one). Sill formation occurs only for a specific range of  
447 dimensionless temperatures  $\theta$  and fluxes  $\phi$ :  $\theta_{min} \leq \theta \leq \theta_{max}$ , where  $\theta_{min} = 0.0039\phi + 0.61$   
448 and  $\theta_{max} = 0.019\phi + 0.68$ . The thermal conditions ( $\theta$ ) depend on injection temperature  $T_i$ , and  
449 dynamical conditions ( $\phi$ ) depend on injection flux  $Q$  and rigidity contrast of the intruded solid.  
450 Therefore, in our experiments, sill formation along an interface depends on three critical param-  
451 eters : the injection temperature  $T_i$ , the injection flux  $Q$ , and the rigidity of the rocks below this  
452 interface.

### Acknowledgements

The authors would like to thank two anonymous reviewers whose comments have strengthened and improved the manuscript. L.C. was supported by a Fellowship from the French Ministry of Higher Education and Research (Ministre de l'Enseignement Suprieur et de la Recherche, MESR), and T.M. acknowledges support from a chaire mixte IRD-UBP. This is Laboratory of Excellence ClerVolc contribution no. XX.

### References

### References

- Annen, C., Sparks, R. S. J., 2002. Effects of repetitive emplacement of basaltic intrusions on thermal evolution and melt generation in the crust. *Earth and Planetary Science Letters* 203, 937–955.
- Benn, K., Roest, W. R., Rochette, P., Evans, N. G., Pignotta, G. S., 1999. Geophysical and structural signatures of syntectonic batholith construction: the South Mountain Batholith, Meguma Terrane, Nova Scotia. *Geophysical Journal International* 136, 144–158.

- Bevington, P., Robinson, D. K., 2003. *Data Reduction and Error Analysis for the Physical Sciences*. McGraw-Hill, New York.
- Bolchover, P., Lister, J. R., 1999. The effect of solidification on fluid-driven fracture, with application to bladed dykes. *Proceedings of the Royal Society of London. Series A: Mathematical, Physical and Engineering Sciences* 455 (1987), 2389–2409.
- Burchardt, S., 2008. New insights into the mechanics of sill emplacement provided by field observations of the Njardvik Sill, Northeast Iceland. *Journal of Volcanology and Geothermal Research* 173, 280–288.
- Cartwright, J., Hansen, D. M. I., 2006. Magma transport through the crust via interconnected sill complexes. *Geology* 34 (11), 929–932.
- Corry, C. E., 1988. Laccoliths; mechanics of emplacement and growth. *Geological Society of America Special Papers* 220, 1–114.
- Crisp, J., 1952. The Use of Gelatin Models in Structural Analysis. *Proceeding IB of the Institute of Mechanical Engineers* 12, 580–604.
- Delaney, P. T., Pollard, D. D., 1981. Deformation of host rocks and flow of magma during growth of minette dikes and breccia-bearing intrusions near Ship Rock, New Mexico. *US Government Printing Office*.
- Galland, O., Cobbold, P. R., Hallot, E., de Bremond d' Ars, J., Delavaud, G., 2006. Use of vegetable oil and silica powder for scale modelling of magmatic intrusion in a deforming brittle crust. *Earth and Planetary Science Letters* 243 (3-4), 786–804.
- Gudmundsson, A., 2011. Deflection of dykes into sills at discontinuities and magma-chamber formation. *Tectonophysics* 500 (1-4), 50–64.
- Horsman, E., Morgan, S., de Saint-Blanquat, M., Habert, G., Nugent, A., Hunter, R. a., Tikoff, B., 2010. Emplacement and assembly of shallow intrusions from multiple magma pulses, Henry

- Mountains, Utah. *Earth and Environmental Science Transactions of the Royal Society of Edinburgh* 100, 117–132.
- John, B. E., 1988. Structural reconstruction and zonation of a tilted mid-crustal magma chamber: The felsic Chemehuevi Mountains plutonic suite. *Geology* 16, 613–617.
- Kavanagh, J. L., Menand, T., Daniels, K., 2013. Gelatine as a crustal analogue: Determining elastic properties for modelling magmatic intrusions. *Tectonophysics* 582, 101–111.
- Kavanagh, J. L., Menand, T., Sparks, R. S. J., 2006. An experimental investigation of sill formation and propagation in layered elastic media. *Earth and Planetary Science Letters* 245 (3-4), 799–813.
- Kavanagh, J. L., Sparks, R. S. J., 2011. Insights of dyke emplacement mechanics from detailed 3D dyke thickness datasets. *Journal of the Geological Society* 168, 965–978.
- Leuthold, J., Müntener, O., Baumgartner, L. P., Putlitz, B., Ovtcharova, M., Schaltegger, U., 2012. Time resolved construction of a bimodal laccolith (Torres del Paine, Patagonia). *Earth and Planetary Science Letters* 325-326, 85–92.
- Lister, J. R., 1999. Fluid-mechanical models of the interaction between solidification and flow in dykes. *Physics and chemistry of dykes*, 115–124.
- Maccaferri, F., Bonafede, M., Rivalta, E., 2010. A numerical model of dyke propagation in layered elastic media. *Geophysical Journal International* 180 (3), 1107–1123.
- Macdonald, G. A., Finch, R. H., 1950. The June 1950 eruption of Mauna Loa, Part II. *The Volcano Letter* 509, 1–6.
- Menand, T., 2008. The mechanics and dynamics of sills in layered elastic rocks and their implications for the growth of laccoliths and other igneous complexes. *Earth and Planetary Science Letters* 267, 93–99.



- Menand, T., 2011. Physical controls and depth of emplacement of igneous bodies: A review. *Tectonophysics* 500 (1-4), 11–19.
- Menand, T., Daniels, K. A., Benghiat, P., 2010. Dyke propagation and sill formation in a compressive tectonic environment. *Journal of Geophysical Research: Solid Earth* (1978–2012) 115 (B8).
- Miller, C. F., Furbish, D. J., Walker, B. a., Claiborne, L. L., Koteas, G. C., Bleick, H. a., Miller, J. S., 2011. Growth of plutons by incremental emplacement of sheets in crystal-rich host: Evidence from Miocene intrusions of the Colorado River region, Nevada, USA. *Tectonophysics* 500, 65–77.
- Muirhead, J. D., Airoidi, G., Rowland, J. V., White, J. D. L., 2012. Interconnected sills and inclined sheet intrusions control shallow magma transport in the Ferrar large igneous province, Antarctica. *Geological Society of America Bulletin* 124 (1-2), 162–180.
- Parsons, T., Sleep, N. H., Thompson, G. A., 1992. Host rock rheology controls on the emplacement of tabular intrusions: Implications for underplating of extending crust. *Tectonics* 11 (6), 1348–1356.
- Richards Jr, R., Mark, R., 1966. Gelatin models for photoelastic analysis of gravity structures. *Experimental Mechanics* 6 (1), 30–38.
- Taisne, B., Jaupart, C., 2009. Dike propagation through layered rocks. *Journal of Geophysical Research: Solid Earth* (1978–2012) 114 (B9).
- Taisne, B., Tait, S., 2009. Eruption versus intrusion? Arrest of propagation of constant volume, buoyant, liquid-filled cracks in an elastic, brittle host. *Journal of Geophysical Research* 114 (B6), B06202.
- Taisne, B., Tait, S., 2011. Effect of solidification on a propagating dike. *Journal of Geophysical Research* 116 (B1), B01206.

- Thordarson, T., Self, S., 1993. The Laki (Skaftar Fires) and Grimsvötn eruptions in 1783-1785. *Bulletin of Volcanology* 55, 233–263.
- Timoshenko, S. P., Goodier, J. N., 1970. *Theory of Elasticity*. McGraw-Hill, New York.
- Traversa, P., Pinel, V., Grasso, J. R., 2010. A constant influx model for dike propagation : Implications for magma reservoir dynamics. *Journal of Geophysical Research* 115 (B1), 1–18.
- White, R. S., Drew, J., Martens, H. R., Key, J., Soosalu, H., Jakobsdóttir, S. S., 2011. Dynamics of dyke intrusion in the mid-crust of Iceland. *Earth and Planetary Science Letters* 304 (3-4), 300–312.

### Captions of figures and tables

FIGURE 1: Experimental apparatus.

The gelatine solid has two layers of different stiffness, to create a priori favourable conditions to form sills. Vegetable oil is heated with a bain-marie and injected at a constant rate with a peristaltic pump in the layered gelatine solid.

FIGURE 2: Experimental intrusions.

(A) Experimental dyke blocked at the interface, experiment 11, three-quarter view. (B) Experimental sill, experiment 1, side view. (C) Experimental dyke passing through the interface, experiment 2, three-quarter view. The dyke takes a triangular shape above the interface.

FIGURE 3: Schematic diagram illustrating the formation of experimental intrusions.

(A) Initial circular dyke, front view. (B) The dyke stops at the interface between the two layers and propagation continues laterally beneath the interface, front view. (C), (D) and (E) are the final shapes of the three different intrusions observed in the experiments. (C) Final shape of the dyke stopping at the interface, front view. (D) The dyke fractures the gelatine at the interface and creates a sill, side view. (E) The dyke pierces the interface, propagates into the upper layer of gelatine and creates a dyke passing through the interface, front view. The dyke takes a triangular shape above the interface.

FIGURE 4: Morphologies of intrusions.

(A) Plumose structures on the feeder dyke, experiment 7, front view. (B) En-echelon segments at the upper tip of the dyke, experiment 14, top view. (C) Lobes on the side of the dyke, experiment 14, side view. (D) Smooth surface and asperity filled by gelatine on a sill, experiment 1, top view. (E) Discontinuities at the edge of the sill, experiment 5, side view.

FIGURE 5: Dimensionless temperature  $\theta$  as a function of dimensionless flux  $\phi$ .

Gray area shows natural ranges of values for  $\theta$  and  $\phi$  as defined in 2.5. Stars represent experiments where no propagation occurred; squares are dykes blocked at the interface; disks are sills; triangles are dykes passing through the interface. Lines (a), (b) and (c) delimit the areas for each type of intrusions. The dashed line (a) is only qualitative whereas the continuous lines (b) and (c) can be determined reliably. See text for details.

FIGURE 6: Sill with its feeder dyke in the Henry Mountains, Utah, USA, modified from [Menand \(2011\)](#).

The view is from the East. The sill, its feeder dyke (both outlined by dashed white lines) and the intruded layered sandstone (continuous white lines) have all been rotated almost  $90^\circ$ . The feeder dyke crosses several similar interfaces before spreading as a sill.

TABLE 1: Behaviour of the dimensionless temperature  $\theta$  and dimensionless flux  $\phi$ .

TABLE 2: Experimental data for investigation of sill formation.

$\theta$  is calculated from equation (4) with  $T_s = 31^\circ \text{C}$ .  $\phi$  is calculated from equation (7) with  $\Delta\rho = 100$ ,  $g = 9.81 \text{ m.s}^{-1}$ ,  $\kappa = 1.4 \times 10^{-7} \text{ m}^2.\text{s}^{-1}$ .  $E$  of the lower gelatine layer is determined and calculated from equation (3). The uncertainties  $\sigma_\theta$  and  $\sigma_\phi$  were calculated according to the principles of the "Propagation of Errors" ([Bevington and Robinson, 2003](#)).

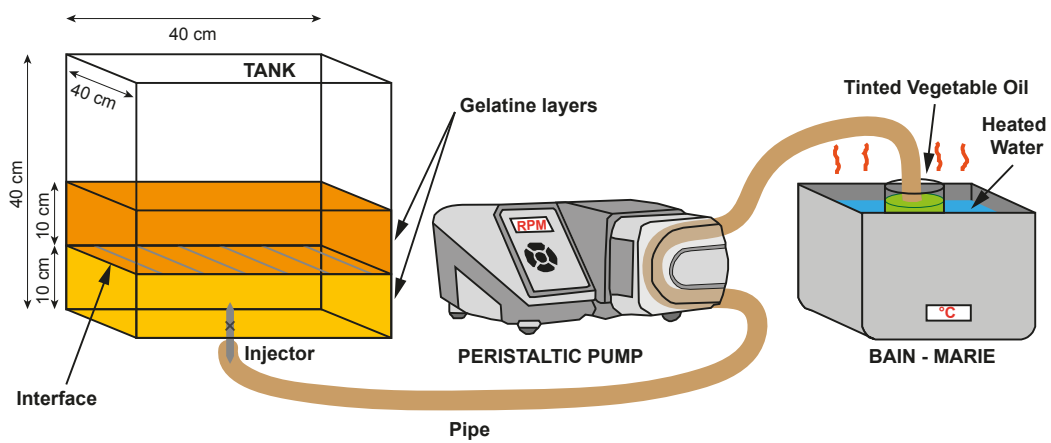


Figure 1: Experimental apparatus.

The gelatine solid has two layers of different stiffness, to create a priori favourable conditions to form sills. Vegetable oil is heated with a bain-marie and injected at a constant rate with a peristaltic pump in the layered gelatine solid.

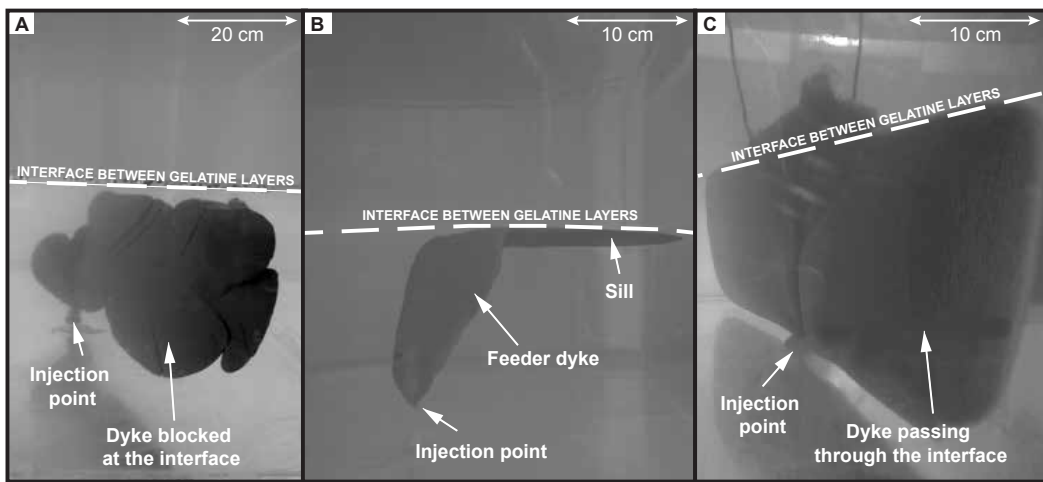


Figure 2: Experimental intrusions.

(A) Experimental dyke blocked at the interface, experiment 11, three-quarter view. (B) Experimental sill, experiment 1, side view. (C) Experimental dyke passing through the interface, experiment 2, three-quarter view. The dyke takes a triangular shape above the interface.

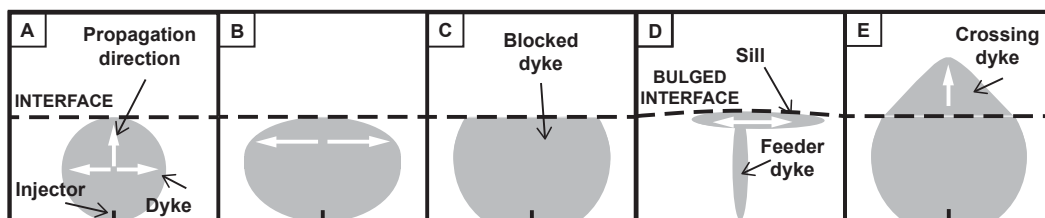


Figure 3: Schematic diagram illustrating the formation of experimental intrusions.

(A) Initial circular dyke, front view. (B) The dyke stops at the interface between the two layers and propagation continues laterally beneath the interface, front view. (C), (D) and (E) are the final shapes of the three different intrusions observed in the experiments. (C) Final shape of the dyke stopping at the interface, front view. (D) The dyke fractures the gelatine at the interface and creates a sill, side view. (E) The dyke pierces the interface, propagates into the upper layer of gelatine and creates a dyke passing through the interface, front view. The dyke takes a triangular shape above the interface.

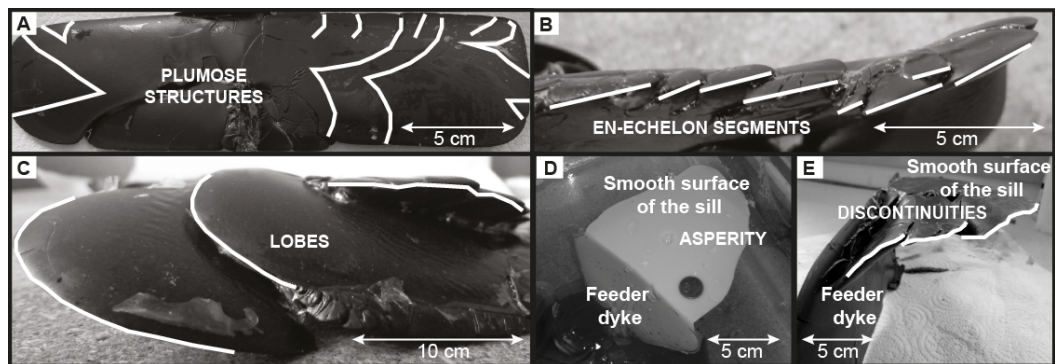


Figure 4: Morphologies of intrusions.

(A) Plumose structures on the feeder dyke, experiment 7, front view. (B) En-echelon segments at the upper tip of the dyke, experiment 14, top view. (C) Lobes on the side of the dyke, experiment 14, side view. (D) Smooth surface and asperity filled by gelatine on a sill, experiment 1, top view. (E) Discontinuities at the edge of the sill, experiment 5, side view.



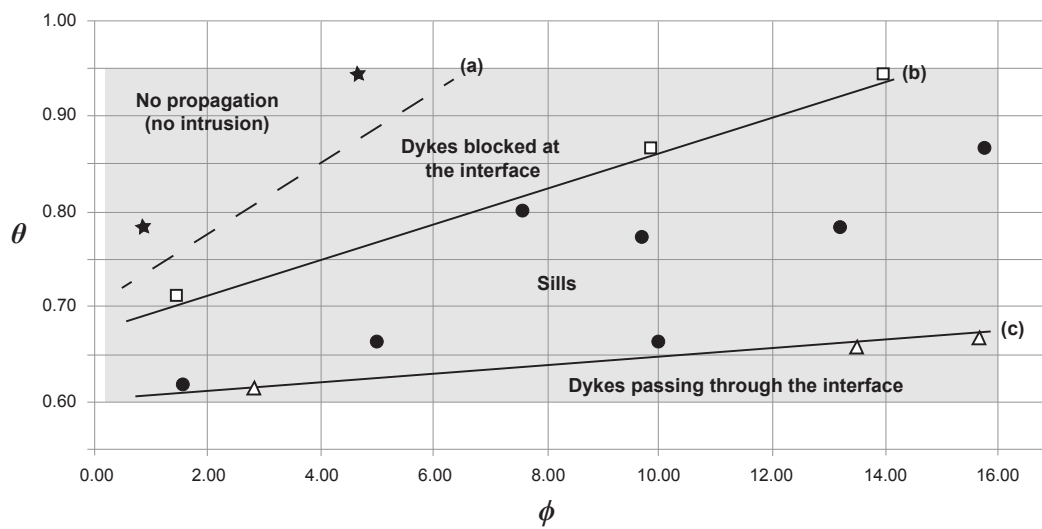


Figure 5: Dimensionless temperature  $\theta$  as a function of dimensionless flux  $\phi$ .

Gray area shows natural ranges of values for  $\theta$  and  $\phi$  as defined in 2.5. Stars represent experiments where no propagation occurred; squares are dykes blocked at the interface; disks are sills; triangles are dykes passing through the interface. Lines (a), (b) and (c) delimit the areas for each type of intrusions. The dashed line (a) is only qualitative whereas the continuous lines (b) and (c) can be determined reliably. See text for details.

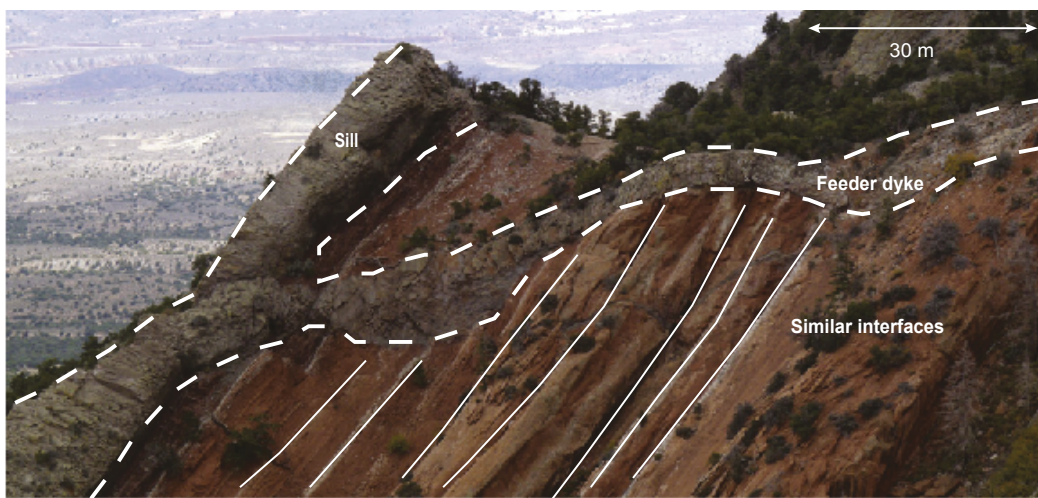


Figure 6: Sill with its feeder dyke in the Henry Mountains, Utah, USA, modified from [Menand \(2011\)](#).

The view is from the East. The sill, its feeder dyke (both outlined by dashed white lines) and the intruded layered sandstone (continuous white lines) have all been rotated almost  $90^\circ$ . The feeder dyke crosses several similar interfaces before spreading as a sill.